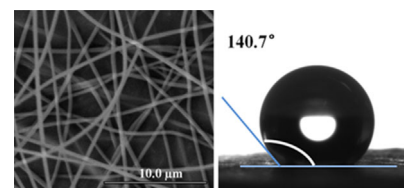


Hydrophobic Electrospun Polyimide Nanofibers for Self-cleaning Materials

Jie Liu,^a Jiangnan Huang,^a Evan K. Wujcik, Bin Qiu, Dan Rutman, Xi Zhang, Enrique Salazard, Suying Wei,^{*} Zhanhu Guo^{*}

In this paper, polyimide (PI) nanofibers with diameters of 300–400 nm are successfully produced via electrospinning methods. Electrospinning parameters such as polymer concentration, applied voltage, feed rate, and the needle-to-collector distance have been studied systematically to investigate their effects on morphology. The smooth-surfaced uniform nanofibers with diameters ranging from 300 to 400 nm can be obtained at the optimal parameters, further discussed herein. The synthesized PI nanofibers show improved thermal stability and a high hydrophobicity with a maximum contact angle of 140.7° and low surface energy of 3.12 mN · m⁻¹, indicating potential applications as self-cleaning materials, such as solar panel cleaning, window glass cleaning, and cements.



1. Introduction

Polymer nanofibers, which have one-dimensional (1-D) structure, have attracted great interest for decades owing to their excellent physical and chemical properties, as well as their superior mechanical properties (e.g., large specific surface area and flexibility in surface functionalities).^[1–3] Tremendous applications ranging from medicine to energy storage have been reported, in which polymer fibers have

been used in tissue engineering components, drug delivery vehicles, medical textile materials, Li-ion batteries, and photovoltaic cells.^[4–8]

Among all the reported approaches to obtain fibers (e.g., vapor phase oxidation, plasma chemical vapor deposition, phase separation self-assembly, and templates),^[9–12] electrospinning is considered to be a highly valued technique for production of fibers with critical dimension ranging from micrometers to nanometers. This is due to its low cost set-up, simple operation, and simple morphology-controlling characteristics.^[13] The electrospinning apparatus consists of a high voltage power supply, a spinneret and an electrically conductive collector, which can be used to fabricate different kinds of polymer, metal oxide, or ceramic fibers.^[14]

Polyimide (PI), as an important high-performance engineering plastic, has excellent mechanical and thermal stabilities, along with its outstanding dielectric properties and superior chemical resistance. Therefore, it has been widely used in many fields, e.g., Garnier et al.^[15] reported the usage of PI as photoresist after adding sodium dichromate as a photoreactive additive. Novel siloxane containing liquid crystalline PI with substituents (methyl-, chloro-, fluoro-) on mesogenic units have been reported by Ueda and coworkers.^[16] Many efforts have been made to

J. Liu, J. Huang, B. Qiu, D. Rutman, X. Zhang, E. Salazard, Z. Guo
Integrated Composites Laboratory (ICL), Dan F. Smith Department
of Chemical Engineering, Lamar University, Beaumont, Texas,
USA

E-mail: zhanhu.guo@lamar.edu

J. Liu, E. K. Wujcik

Materials Engineering And Nanosensor (MEAN) Laboratory, Dan F.
Smith Department of Chemical Engineering, Lamar University,
Beaumont, Texas, USA

S. Wei

Department of Chemistry and Biochemistry, Lamar University,
Beaumont, Texas, USA

E-mail: suying.wei@lamar.edu

^aBoth the authors contributed equally to this work.

improve the properties of PI due to the increasing requirements for advanced applications. A growing interest in PI over the past two decades has arisen in its application in gas separation membranes.^[17] For instance, in 1962 DuPont (USA) initially developed commercial PI membranes to separate helium from natural gas.^[18] Another notable example includes the preparation of PI Langmuir–Blodgett (LB) films and their interfacial and storage phenomena investigation reported by Kastner et al.^[19] Still other applications include proton conductive membranes for fuel cells, proton-exchange-membrane, and carbon dioxide plasticization reduction.^[20–22]

It has been found that electrospun PI nanofibers have remarkably better mechanical properties than those made of other polymers, such as Nylon, Nomex, polyacrylonitrile (PAN), polylactide (PLA), etc.^[23,24] Electrospun nanofibers have also been found to be ideal candidates for reinforcing polymer materials and lightweight materials.^[25] Herein, an electrospinning method was used to fabricate PI nanofibers. The fabricated PI nanofibers have been systematically studied, by varying the different parameters and observing their effects on the morphology of PI nanofibers. It was found that the size distribution of PI nanofibers can be controlled through adjusting the parameters, such as tip-to-collector distance, voltage applied, flow rate, and concentration percentage of the solution. Solvent effects on the thermal stability and hydrophobic properties of the synthesized PI nanofibers were studied as well.

2. Experimental Section

2.1. Materials

Polyimide (PI, powder, Matrimid 5218 US) was purchased from Huntsman Advanced Materials Americas, Inc. *N*-methyl-2-pyrrolidone (NMP) (Acros Organics, NJ, USA: 1–800-ACROS-01) and anhydrous *N,N*-dimethylformamide (DMF) (Acros Organics, NJ, USA: 1–800-ACROS-01) were used as received without further treatment.

2.2. Preparation of Polymer Solutions

The standard procedure for preparation of PI/NMP solutions was as follows. PI was dissolved in the solvent of *N*-methyl-2-pyrrolidone (NMP). Then, the solution was vigorously magnetically stirred (400 rpm) overnight in a 50 mL glass beaker sealed by aluminum foil and Parafilm at room temperature. The PI concentrations were varied: 5.0, 8.0, 10.0, 15.0, and 20.0 wt.-%. The specific amount of PI/DMF solution (15.0 wt.-%) was obtained by similar methods. All of the PI/NMP and PI/DMF solutions were used for fabricating the electrospun nanofibers.

2.3. Fabrication of PI/NMP and PI/DMF Fibers

The PI/NMP and PI/DMF fibers were fabricated by an electrospinning method, outlined hereafter. The electrospinning

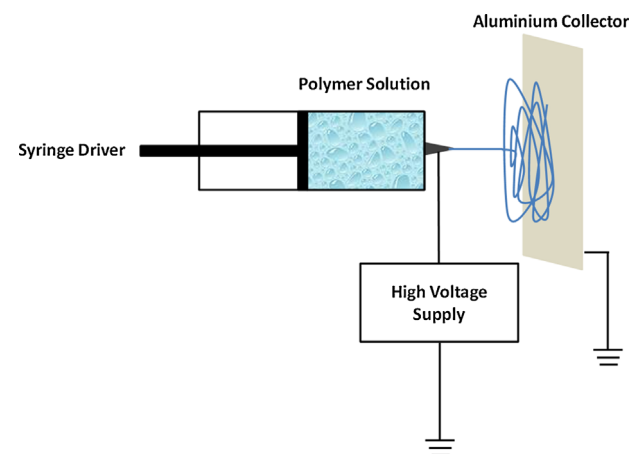
apparatus consist of a high voltage supply (Gamma High Voltage Research, Product HV power, Model No. ES3UP-5w/DAM), a syringe pump (NE-300, New Era Pump Systems, Inc.), a 5 mL syringe and a flat piece of aluminum foil (as both the grounded counter electrode and collector). The schematic diagram of the setup is shown in Figure 1. The viscous solution is first loaded in the syringe with a stainless steel gauge needle, which is connected to high voltage supply to provide a negatively polarized DC voltage up to 30.0 kV. A flat piece of aluminum foil is used as a collector for the fibers. The feed rate of the solution is controlled by the syringe pump. The feed rates were studied at 2.0, 4.0, and 8.0 $\mu\text{L}\cdot\text{min}^{-1}$, respectively. The working voltages in this study were controlled at 15.0, 20.0, and 25.0 kV. Through the needle, the external electrical field of high voltage applied to the polymer solution can overcome the surface tension of the viscous solution to form a polymer solution jet, which accumulates on the aluminum foil collector in the form of fibers. The fibers were then dried at room temperature and atmospheric pressure overnight for further characterization.

2.4. Fabrication of PI Samples for Contact Angle Test

PI powders were pressed into a round disk by a press molding machine (Carver 3853–0, USA) at room temperature. The procedure was as follows. The PI powders were put into a cylinder mold, which was then placed in the molding machine between two panels. The mold was maintained at room temperature for 6 h under 10 MPa pressure. The PI film and nanofibers were secured to the top of paper without further treatment and then used for the contact angle test.

2.5. Characterization

The morphology of the fibers, which were obtained from PI/NMP and PI/DMF solutions, was investigated by scanning electron microscopy (Hitachi S-3400 scanning electron microscopy). The rheological behavior of the polymer solutions under different



■ Figure 1. A schematic diagram of an electrospinning setup.

concentrations were evaluated with an AR 2000ex Rheometer (TA Instrumental Company) at a shear rate range from 1 to 100 L/s at 25 °C. A series of measurements were carried out in a corn-and-plate geometry with a diameter of 40 mm and a truncation of 66 μm . Fourier transform infrared spectroscopy (FT-IR, Bruker Inc. Vector 22 FT-IR spectrometer, coupled with an ATR accessory) was used to characterize the functional groups of the synthesized PI fibers, PI powders, and PI films from the polymer solutions over the range of 4 000–50 cm^{-1} at a resolution of 4 cm^{-1} .

The thermal stabilities of the electrospun PI fibers, PI powders, and films were studied with a thermogravimetric analysis (TGA, TA instrument, TGA Q-500). TGA curves were recorded from 25 to 900 °C under 60 $\text{mL} \cdot \text{min}^{-1}$ flow of nitrogen and air, respectively, at a heating rate of 10 °C $\cdot \text{min}^{-1}$.

The wettability of PI powder disk, PI film, and nanofibers (fabricated from the PI/NMP and PI/DMF solutions) was determined by the sessile drop technique (Contact angle analyzer, Future Digital Scientific Corp.), using deionized water as the liquid.

3. Results and Discussion

3.1. Morphology of the PI Fibers

Here, electrospinning methods were used to fabricate PI fibers, and the effects of important parameters, such as the PI concentration, applied electrical voltage, tip-to-target distance and feed rate of the polymer solution, on the morphologies of polymer fibers were systematically studied.

3.1.1. Polyimide Concentration Effect

The SEM micrographs of the pure electrospun PI fibers, fabricated from the solutions with a loading of 5.0, 8.0, 10.0, 15.0, and 20.0 wt.-% PI are shown in Figure 2. Figure 2a shows only round disks with the diameter ranging from 2 000 to 3 000 nm, when the PI loading is 5.0 wt.-%. With the concentration of PI solution of 8.0 wt.-%, particles with random diameters connected by some ultrafine fibers are observed (Figure 2b). The 10.0 wt.-% PI solution, bunched fibers with beads are observed (Figure 2c). However, when the concentration increases to 15.0 wt.-% PI, uniform, continuous, and smooth surfaced PI nanofibers with the diameter of 300–400 nm are observed (Figure 2d). At the concentration of 20.0 wt.-%, shown in Figure 2e, the diameters of the fibers reach 1 500–2 000 nm in average, and the surface of the collected fibers remains smooth. The above observations indicate that the concentration of polymer solution plays an important role in forming uniform nanofibers with a smooth surface. This can be explained by relating the surface tension, viscoelastic force, and the electrostatic repulsions of the dynamic system. When these reach a balance, a stable jet is formed at the spinneret tip to obtain high quality fibers.^[5,26] Significant bead formation will occur if this jet is unstable and the electrospinning parameters are not optimized.^[8,27] With an increasing polymer concentration (and hence, increasing viscosity), the viscoelastic force, as the dominating force on

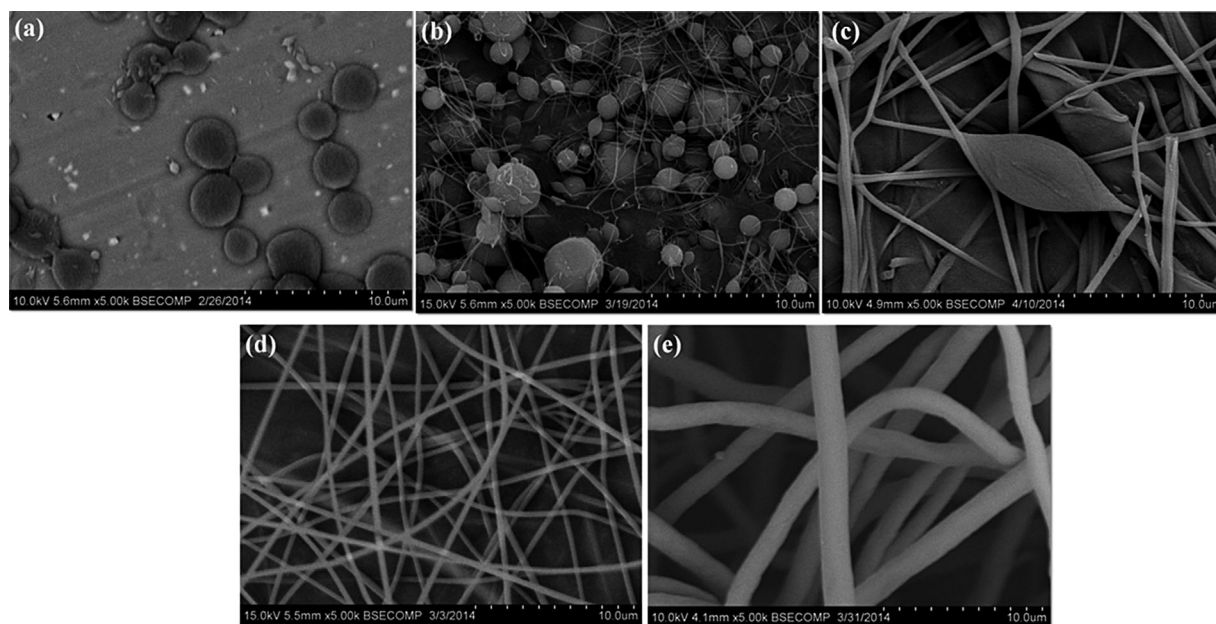


Figure 2. SEM images of PI fibers electrospun from NMP solutions with a PI loading of (a) 5.0, (b) 8.0, (c) 10.0, (d) 15.0, and (e) 20.0 wt.-% (15.0 cm, 2.0 $\mu\text{L} \cdot \text{min}^{-1}$ and 20.0 kV).

the fluid, favors the formation of bead-free nanofibers with smooth surface.^[5]

3.1.2. Applied Voltage Effect

Figure 3 shows the pure PI fibers electrospun from a 15.0 wt.-% polymer solution with a varied applied voltage of 15.0, 20.0, and 25.0 kV. The working distance and feed rate were maintained constant at 15.0 cm and $2.0 \mu\text{L} \cdot \text{min}^{-1}$, respectively. Figure 3a shows the fibers at 15.0 kV with uniform diameter about 400–500 nm and a smooth surface. In contrast, straight fibers at 20.0 kV (Figure 3b and c) exhibit smooth surfaces with diameters of 300–400 nm. This shows that the applied voltage has no significant effect on the morphology of fibers over the range of 15.0–20.0 kV.

However, when the voltage increases to 25.0 kV, the fibers are observed to change from straight to curved orientations and the diameters range widely from 200 to 800 nm. This is in agreement with previous reports^[26,27] that higher voltages favor the formation of uniform and smooth nanofibers only under 20.0 kV.^[8]

3.1.3. Feed Rate Effect

Figure 4 shows SEM micrographs of the nanofibers fabricated from the 15.0 wt.-% PI/NMP solution, with a varying feed rate of 2.0, 4.0, and $8.0 \mu\text{L} \cdot \text{min}^{-1}$, at a voltage of 20.0 kV. At $2.0 \mu\text{L} \cdot \text{min}^{-1}$, the fabricated PI fibers show uniform diameters about 300–400 nm and straight structure with smooth surface (Figure 4a and b). When the feed

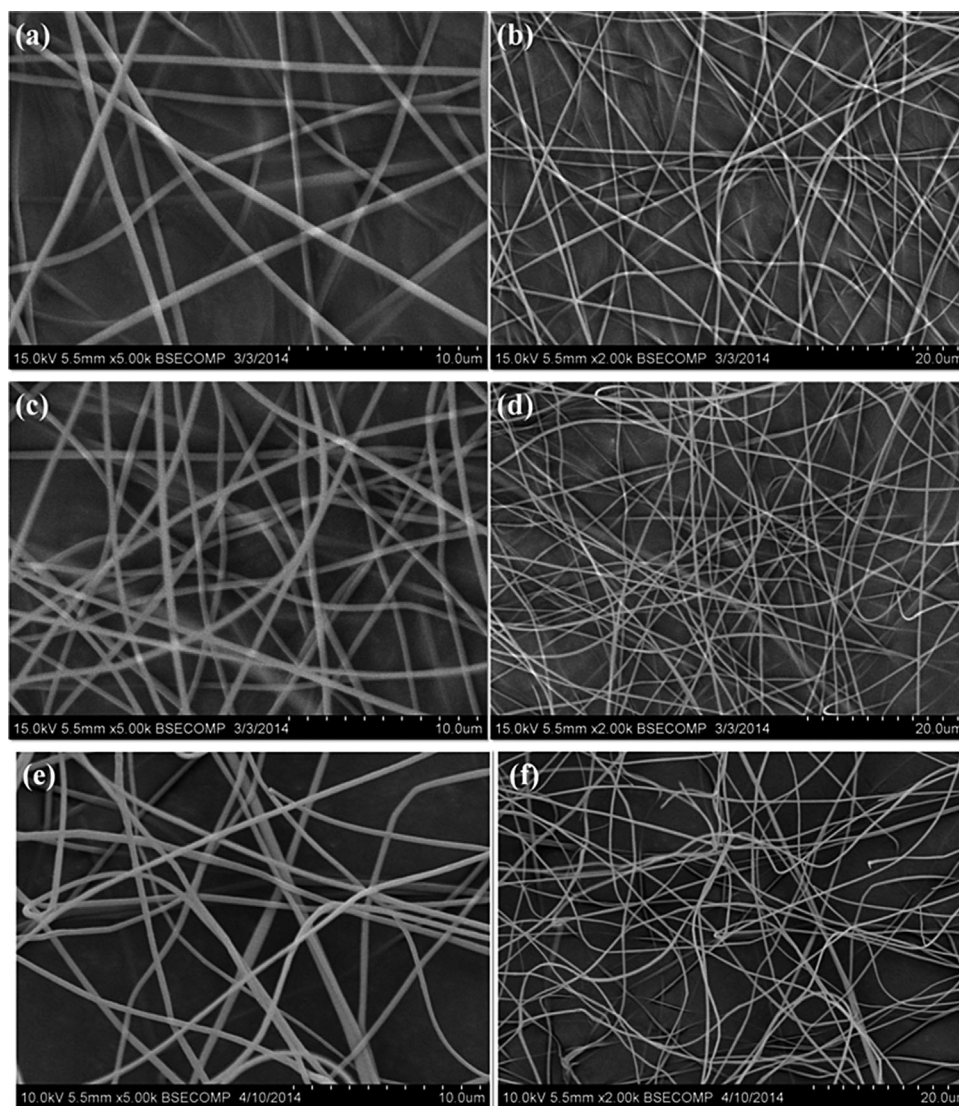


Figure 3. SEM images of the PI fibers electrospun from 15.0 wt.-% PI/NMP solutions at a voltage of (a and b) 15.0, (c and d) 20.0, and (e and f) 25.0 kV (operational parameters: 15.0 cm working distance and $2.0 \mu\text{L} \cdot \text{min}^{-1}$ feed rate).

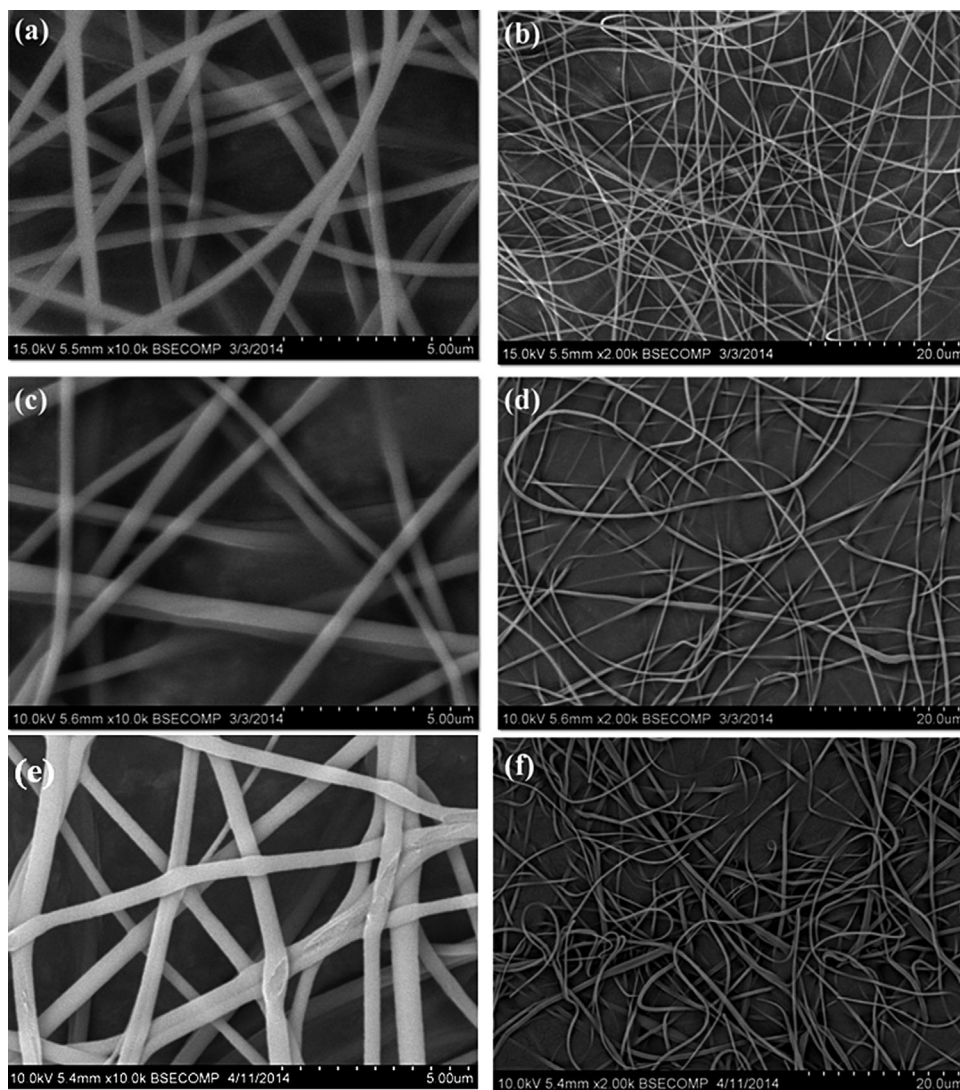


Figure 4. SEM micrographs of PI fibers electrospun from the 15.0 wt.-% PI/NMP solution at a feed rate of (a and b) 2.0, (c and d) 4.0, and (e and f) 8.0 $\mu\text{L} \cdot \text{min}^{-1}$ (operational parameters: 15.0 cm working distance at 20.0 kV).

rate is raised to 4.0 $\mu\text{L} \cdot \text{min}^{-1}$, the PI fibers have more variable diameters from 200 to 600 nm (Figure 4c and d). As the feed rate is further increased to 8.0 $\mu\text{L} \cdot \text{min}^{-1}$, the fibers gather together to form bunched or bundled structures with their diameters ranging from 500 to 1500 nm (Figure 4e and f). Therefore, a lower feed rate is found to be more desirable for manufacturing uniform fibers with thinner diameters. Contrarily, the higher feed rates lead to thicker fiber formation. This has been shown previously and can be attributed to lower feed rate providing sufficient time for the solvent to evaporate, thus the fibers are able to form uniform nanofibers.^[28] It is well known that reduction in the diameter and quantity of defects will improve the strength of fibers, so fibers in small size are usually adopted

by manufacturers because of their technologically and economically feasibility.^[29]

3.1.4. Working Distance Effect

Figure 5 shows the working distance effect on the pure PI fibers fabricated from 15.0 wt.-% polymer solution under the applied electric voltage of 20.0 kV at a feed rate of 2.0 $\mu\text{L} \cdot \text{min}^{-1}$. The working distances from the needle tip to the collector are chosen as 10.0, 15.0, and 20.0 cm, respectively. With the working distance increasing, the pure PI fibers can maintain very uniform diameters about 400 nm and smooth surface (Figure 5a–f). As mentioned above, the fibers have no significant change in either the morphology

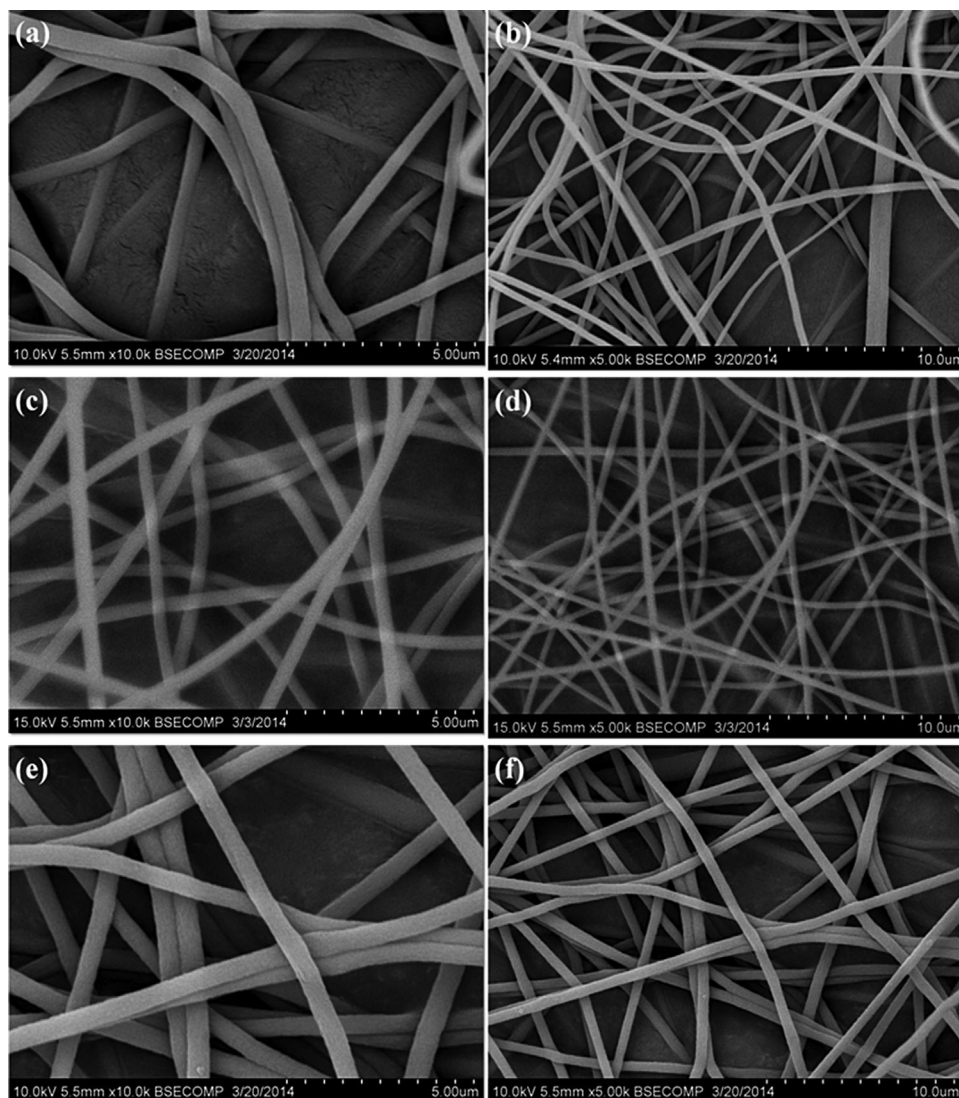


Figure 5. SEM micrographs of the PI fibers electrospun from the 15.0 wt.-% PI/NMP solution with a working distance of (a and b) 10.0, (c and d) 15.0, and (e and f) 20.0 cm, operational parameter: 20.0 kV, 2.0 $\mu\text{L} \cdot \text{min}^{-1}$.

or size distribution as the working distance is varied, which is in accordance with the results from previous report.^[30]

3.1.5. Solvent Effect

In order to determine the solvent effect on the morphology of the PI fibers, DMF was also selected as solvent for comparison. Based on the results discussed above, the optimal experimental parameters are determined as follows: an applied voltage of 20.0 kV, a feed rate of 2.0 $\mu\text{L} \cdot \text{min}^{-1}$, a working distance of 15.0 cm, and a concentration at 15.0 wt.-% PI. Under this condition, both polymer solutions can form stable Taylor cones,^[8,26] which favor the fabrication of uniform nanofibers by this electro-

spinning method. The PI fibers (seen in the Figure 6a and b) electrospun from the PI/NMP solution with the diameter of 300–400 nm are relatively thinner (almost half of the diameter) than the fibers (shown in the Figure 6c and d) electrospun from the PI/DMF solution with a diameter of 600–700 nm, indicating that the NMP has a better effect on forming uniform and fine fibers than DMF. The solvent NMP, being more volatile than DMF, helps to form the thinner electrospun fibers,^[31] which have larger specific surface area. Considering the desirable properties of relatively low flammability, low toxicity and low boiling point, NMP can be a good choice as the solvent for manufacturing thin nanofibers by electrospinning method.

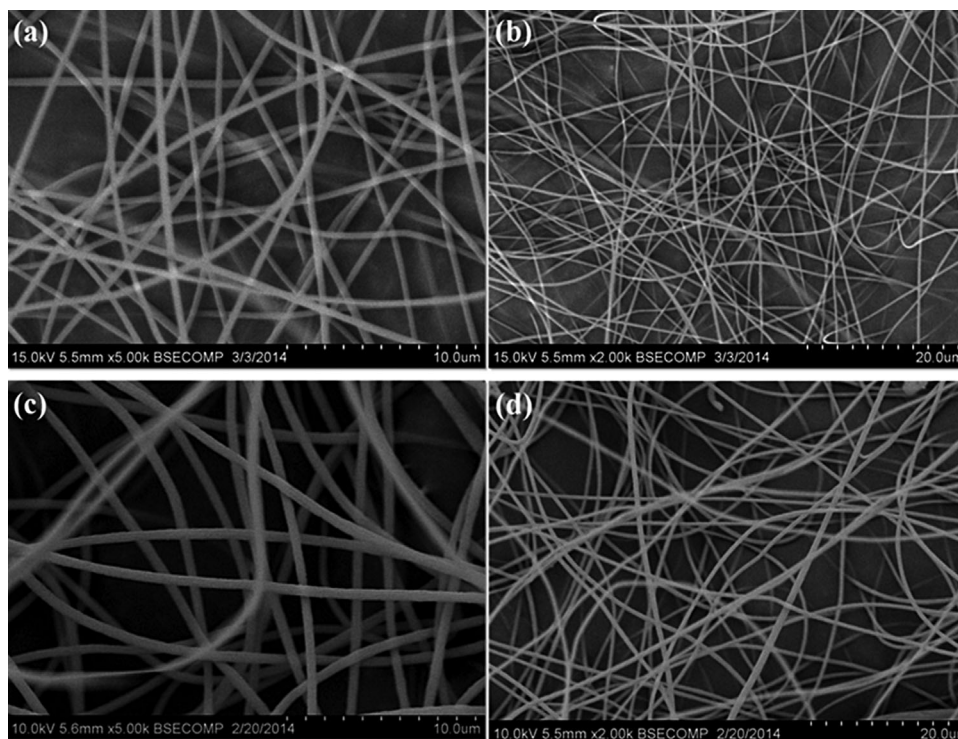


Figure 6. SEM micrographs of PI fibers electrospun from 15.0 wt.-% PI/NMP solution (a and b) and 15.0 wt.-% PI/DMF solution (c and d) (operational parameters: $2.0 \mu\text{L} \cdot \text{min}^{-1}$, 20.0 kV, and 15.0 cm).

3.2. Rheological Characteristics

The rheological characteristics of a fluid can be described by the power law of fluids, Equation (1):

$$\tau = \mu(\dot{\gamma})^n \quad (1)$$

where τ is the shear stress, μ (the dynamic viscosity) the proportionality factor or the flow consistency index, $\dot{\gamma}$ is the shear rate, and n (the exponent of the power law) is the flow behavior index. The value of n determines the fluid type.^[32] The fluid (dilatant fluid) exhibits shear thickening properties, when $n > 1$. For $n < 1$, the fluid (pseudoplastic fluid) exhibits shear thinning properties. For $n = 1$, Newtonian fluid has a linear rate of shear stress versus shear rate.

The rheological data obtained is displayed in Figure 7a and b, which shows the viscosity and shear stress as a function of shear rate for PI/NMP solutions under the concentrations of 5.0, 8.0, 10.0, 15.0, and 20.0 wt.-%. At shear rates ranging from 1.0 to 100 s^{-1} , the average viscosity of the solutions increase steadily from $0.03 \text{ Pa} \cdot \text{s}$ (5.0 wt.-% PI) to $1.63 \text{ Pa} \cdot \text{s}$ (15.0 wt.-% PI) at 25°C . However, the average viscosity of 20.0 wt.-% PI/NMP solution increases dramatically to $12.82 \text{ Pa} \cdot \text{s}$. From Figure 7b, it can be found that the shear stress increases almost linearly with the increasing shear rate, indicating Newtonian behavior. The relative

molecular weight and viscosity of the as-synthesized PI solutions are listed in Table 1.

The exponent (n) of the PI/NMP solutions with PI loadings of 5.0, 8.0, and 10.0 wt.-%, which are higher than 1, indicate a dilatant fluid behavior. With the PI loading increased to 15.0 and 20.0 wt.-%, the exponent values gradually decrease to 0.88 and 0.83, respectively. This illustrates a pseudoplastic nature of the solutions. For non-Newtonian fluid, the orientation of the polymer chains, which is the governing factor, influences the behavior of the fluid.^[33] Therefore, the gradual decreasing values of the exponent displays a trend from dilatant fluid behavior to pseudoplastic. This corresponds to the PI concentration increasing, and can be predicted by the orientation of the polymer segment in varying solutions.

3.3. FT-IR Spectra

Figure 8 shows the FT-IR spectra of the as received PI powders, film (obtained from evaporating the solvent from PI/NMP solution at 80°C in a vacuum) and fibers (from the 15 wt.-% PI/NMP solution) in the wavenumber range of $500\text{--}4000 \text{ cm}^{-1}$. The FT-IR spectra of the as received PI powders are characterized by typical bands at around 1778 cm^{-1} (asymmetric stretch of CO in the imide group), 1718

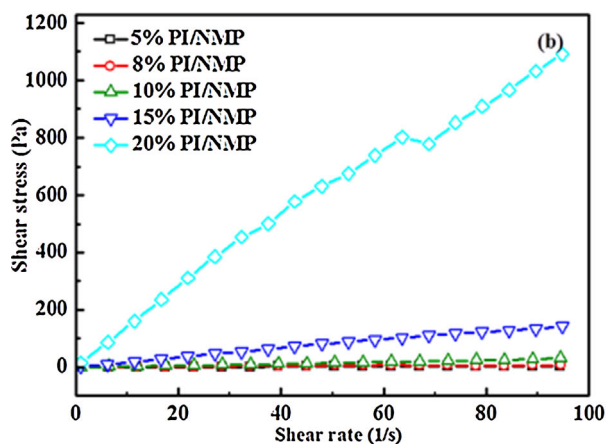
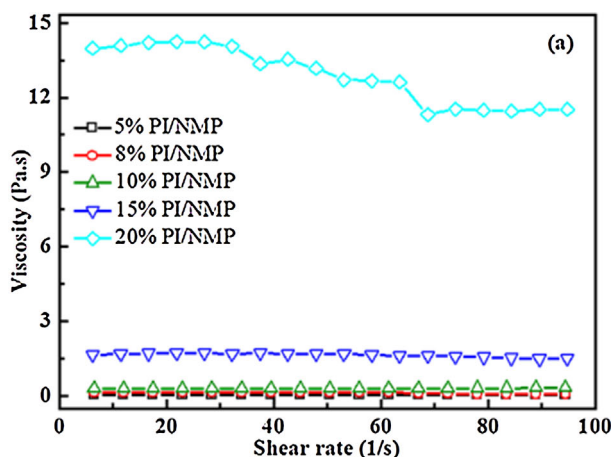


Figure 7. (a) Viscosity and (b) shear stress of the PI/NMP solution with different concentrations: 5.0, 8.0, 10.0, 15.0, and 20.0 wt.-%.

cm^{-1} (symmetric stretch of CO in the imide group), and 1368 cm^{-1} (stretch of C–N in the imide group).^[34] Moreover, the bands at 720 , 825 , and 858 cm^{-1} are attributed to the 1,2,4-trisubstitute of the benzene structure and the bands of 1511 and 1487 cm^{-1} are assigned to the C–C backbone vibration of the benzene ring. Other stretching and vibration of methyl groups can be found in the range of $1000\text{--}1250\text{ cm}^{-1}$. Although, the characteristic bands can also be observed in the spectra of PI fibers and PI film, the signal intensity of imide bands is attenuated significantly.

Table 1. The viscosity of PI/NMP solutions with different loadings.

PI/NMP solution	5.0 wt.-%	8.0 wt.-%	10.0 wt.-%	15.0 wt.-%	20.0 wt.-%
Viscosity [$\text{Pa} \cdot \text{s}$]	0.03	0.12	0.30	1.63	12.82
n	1.12	1.12	1.10	0.88	0.83

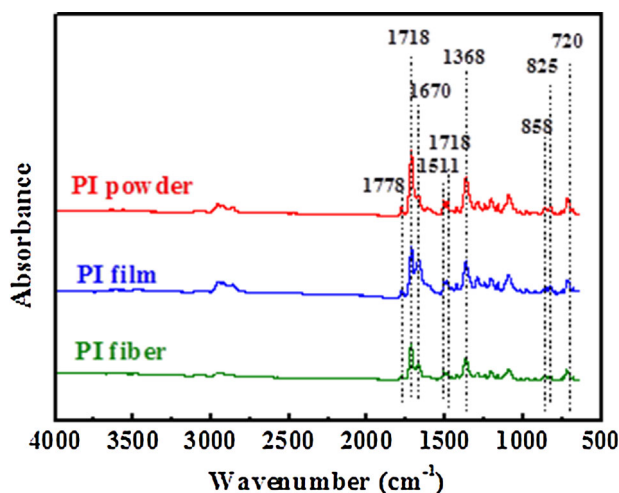


Figure 8. FT-IR spectra of the as received PI powders, PI film, and PI fibers.

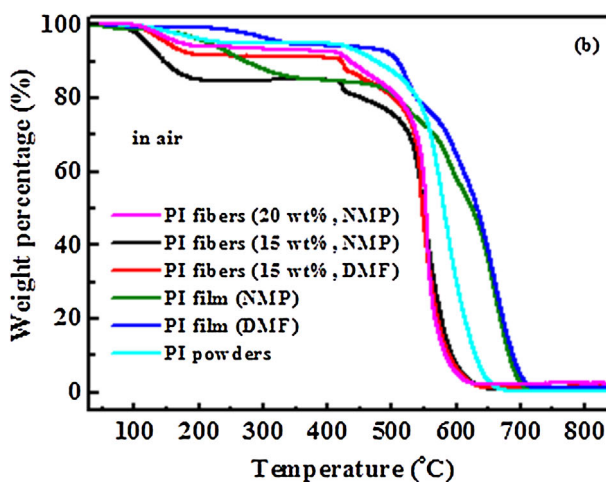
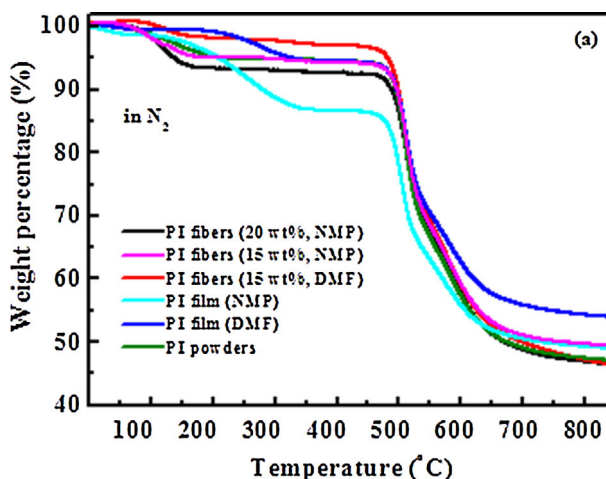


Figure 9. Thermogravimetric curves for all samples in (a) nitrogen and (b) air.

Table 2. TGA results of all the samples in nitrogen.

Samples (in N ₂)	T _{5%} [°C]	Weight residue at 400 °C [%]	Weight residue at 800 °C [%]
PI fibers (20 wt.-%, NMP)	162.4	92.6	46.9
PI fibers (15 wt.-%, NMP)	280.0	94.3	49.7
PI fibers (15 wt.-%, DMF)	495.2	97.1	47.2
PI film (NMP)	230.8	86.7	49.2
PI film (DMF)	343.2	94.6	54.3
PI powders	232.4	94.6	47.4

This indicates that the imide bonds are reduced after being dissolved in NMP.^[31] Furthermore, no additional bands appear in the FT-IR spectra of PI film and PI fibers, compared with the spectrum of typical PI powders, indicating that the molecular structure of the PI maintains consistent besides the quantum size effects.

3.4. Thermogravimetric Analysis (TGA)

Figure 9a and b show the thermal gravimetric curves of all samples in air and nitrogen. From these thermograms, the initial thermal decomposition temperatures $T_{5\%}$ (the weight loss of 5%) and the weight residue at 400 and 800 °C are summarized in Table 2 and Table 3. The obvious weight losses in the 100–200 °C are likely due to solvent effects, as the DMF and NMP boiling points are 153 and 203 °C, respectively. From Figure 10a, PI fibers (15.0 wt.-%, DMF) and PI film (DMF) have the highest decomposition temperature $T_{5\%}$ of 495.2 and 343.2 °C, respectively. And they also show highest weight residue at 400 °C, 97.1% for PI

fibers (15.0 wt.-%, DMF) and 94.6% for PI film (DMF). It is worthy to note that the PI film from the DMF solution holds 54.3% weight loss at 800 °C, indicating its thermal stability at high temperatures in a nitrogen atmosphere. Moreover, all the samples maintain high weight percentage over 46.9% at 800 °C in a nitrogen atmosphere. When these samples are tested in air, the PI film from PI/DMF solution displays excellent thermal stability in the range of 30–400 °C, with the $T_{5\%}$ of 332.2 °C and weight residue of 94.2% at 400 °C. However, the thermal stability of PI nanofibers fabricated from the PI/NMP solution or PI/DMF solution decreases significantly more than the PI powders, because the structure of nanofibers make them more active in air. All the samples are decomposed almost completely at 700 °C in air. It can be observed that both the fibers and films fabricated from the polymer solutions using the DMF as the solvent have more stable thermal properties. The result can be attributed to the fact that DMF is in favor of forming the smoother surfaced structures of fibers and film than the solvent NMP does, which has a great effect on improving the thermal stability.^[31]

Table 3. TGA results of all the samples in air.

Samples (in air)	T _{5%} [°C]	Weight residue at 400 °C [%]	Weight residue at 800 °C [%]
PI fibers (20 wt.-%, NMP)	168.5	92.6	2.4
PI fibers (15 wt.-%, NMP)	118.6	84.8	0.9
PI fibers (15 wt.-%, DMF)	149.8	90.9	1.5
PI film (NMP)	213.1	84.8	1.3
PI film (DMF)	332.2	94.2	1.2
PI powders	245.4	94.7	0.3

3.5. Contact Angle

To evaluate the variation of the surface properties owing to the presence of a nanofiber structure, a contact angle measurement was carried out. The sessile drop method^[35] was used to determine the surface characteristics of different samples from P1 to P6. The optimal parameters for the electrospinning nanofibers were chosen at: a voltage of 20.0 kV; a feed rate of 2.0 $\mu\text{L} \cdot \text{min}^{-1}$; and a working distance of 15.0 cm. Deionized water was used as the test liquid to evaluate the hydrophobic property.^[36] The solvent and morphology effects on the hydrophobicity of PI nanofibers were studied as well. Figure 10 represents the static contact angle images of P1 to P6. The contact angle of

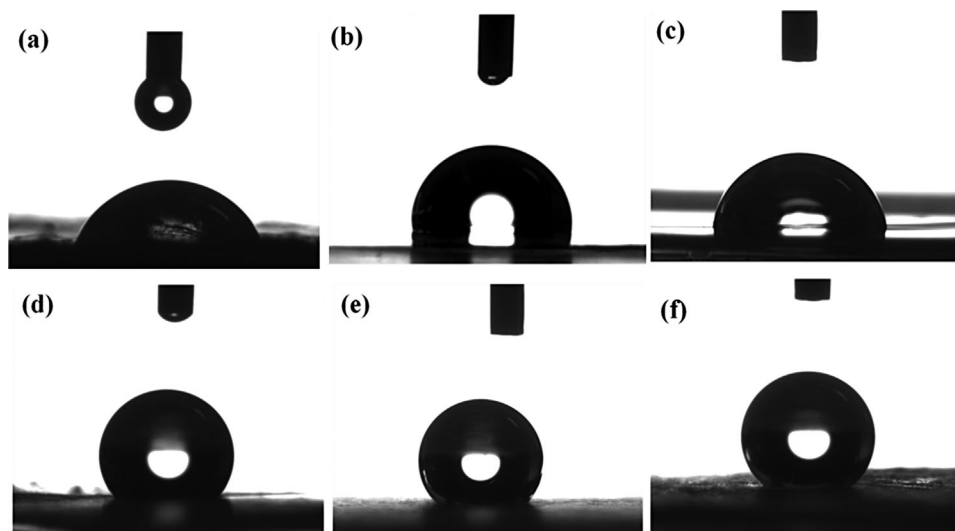


Figure 10. Static contact angle images of water droplet on the surface of (a) as received PI powders (P1), (b) PI film/NMP (P2), (c) PI film/DMF (P3), (d) PI nanofibers (P4) fabricated from 15.0 wt.-% PI/NMP solution, (e) PI nanofibers (P5) fabricated from 15.0 wt.-% PI/DMF solution, (f) PI nanofibers (P6) fabricated from 20.0 wt.-% PI/NMP solution.

P1 is observed to be 73.0° , however, the contact angles of P2 and P3 are 92.0° and 94.2° , respectively. The enhanced hydrophobicity is caused by the increased smoothness of the nanofibers' surface. DMF contributes to the formation of smooth surfaced membrane. Comparatively, when using NMP as the solvent, the membrane has a relatively rough surface.^[31] Moreover, the sample P4 shows an enhanced hydrophobicity, with the contact angle as high as 132.0° , due to the microstructure and large specific surface of the nanofibers. The contact angle of P5 with much thicker diameters is about 134.0° —this is higher than that of the P4. A possible reason for this observation is that the electrospun nanofibers with ultrathin diameter and smooth surface can create a hydrophobic surface due to the high surface tension, on which the high contact angle can drive the water droplet away, indicating the potential applications in the self-cleaning membrane.^[37] In order to investigate the size effect on the contact angle, P6 electrospun from 20.0 wt.-% PI/NMP solution was studied. It is found that contact angle increases (to 140.7°) with the diameter of nanofibers increasing to 1 500–2 000 nm.

The contact angle is defined by the equilibrium of a liquid drop on a solid surface under three interfacial tensions:

liquid–vapor γ_{lv} , solid–vapor γ_{sv} , and solid–liquid γ_{sl} . Here, the Neumann's equation of state^[38–40] is used to calculate the surface energy of the solid for certain liquid, with the given surface tension of a liquid ($\gamma_{(H_2O)} = 72.75 \text{ (mN} \cdot \text{m}^{-1}\text{)}$) and measured contact angle. Neumann's Equation of state can be expressed as:

$$\cos\theta = 2 \cdot \sqrt{\frac{\gamma_g}{\gamma_l}} \cdot e^{-\beta(\gamma_l - \gamma_g)^2} - 1 \quad (2)$$

where β is a constant with the average value of $0.0001247 \text{ (m}^2 \cdot \text{mJ}^{-1}\text{)}^2$, which is determined by the experimental contact angles on the surfaces of different kinds of solids; γ_s ($\text{mN} \cdot \text{m}^{-1}$) is the surface energy of solid, which is calculated from the equation; γ_l ($\text{mJ} \cdot \text{m}^{-2}$) is the surface tension of liquid vapor, which is given for a certain type of liquid; θ is the Young contact angle measured on certain type of solid surface.^[40,41] The calculated surface energies of different PI samples are listed in Table 4. From the data in the table, it can be found that the surface energy gradually decreases to $3.12 \text{ mN} \cdot \text{m}^{-1}$ from $39.81 \text{ mN} \cdot \text{m}^{-1}$, with the contact angles increasing from 73° to 140.7° . Among them, the PI fibers electrospun from 20 wt.-% PI/NMP solution has the lowest

Table 4. The contact angles and surface energies of all samples.

Sample	(a) PI powders	(b) PI film (NMP)	(c) PI film (DMF)	(d) PI fiber (15 wt.-%, NMP)	(e) PI fiber (15 wt.-%, DMF)	(f) PI fiber (20 wt.-%, NMP)
Contact angle [$^\circ$]	73.0	92.0	94.2	132.0	136.0	140.7
Surface energy [$\text{mN} \cdot \text{m}^{-1}$]	39.81	27.95	26.58	6.04	4.57	3.12

surface energy of $3.12 \text{ mN} \cdot \text{m}^{-1}$, with the highest contact angle of 140.7° . This demonstrates that the hydrophobicity has been greatly enhanced, as compared to the PI powders and the PI film. A material with these properties will have great potential applications in the field of self-cleaning materials.

4. Conclusion

By electrospinning methodologies, we have successfully synthesized PI nanofibers with smooth surface and a uniform diameter of 300–400 nm, by studying the operational effects on their morphology, such as concentration, applied voltage, working distance, and feed rate. The optimal parameters were found to be at a voltage of 20.0 kV, a feed rate of $2.0 \mu\text{L} \cdot \text{min}^{-1}$, a working distance of 15.0 cm and a concentration at 15.0 wt.-% PI. The optimized electrospun PI nanofibers show greatly improved thermal stability for their thin diameters from the TGA test, and maintain consistent molecular structure from the FT-IR. Moreover, the electrospun PI nanofibers fabricated from the PI/NMP solution illustrate a high hydrophobicity, having a contact angle of 140.7° and a low surface energy of $3.12 \text{ mN} \cdot \text{m}^{-1}$, indicating the potential applications in self-cleaning materials,^[15] such as tiles, facades, and glass panes used in building materials, which will consequently lower the consumption of energy and chemical detergents.

Acknowledgement: This project is financially supported by a Research Enhancement Grant from Lamar University. Partial support is also acknowledged from the National Science Foundation-Chemical and Biological Separation under the EAGER program (CBET 11–37441) managed by Dr Rosemarie D. Wessonis.

Received: August 28, 2014; Revised: October 30, 2014; Published online: January 3, 2015; DOI: 10.1002/mame.201400307

Keywords: electrospun; materials; nanofiber; polyimide; self-cleaning

- [1] Z. M. Huang, Y. Z. Zhang, M. Kotaki, S. Ramakrishna, *Compos. Sci. Technol.* **2003**, *63*, 2223.
- [2] B. Ding, M. Yamazaki, S. Shiratori, *Sens. Actuators, B: Chem.* **2005**, *106*, 477.
- [3] J. Zhu, S. Wei, J. Ryu, M. Budhathoki, G. Liang, Z. Guo, *J. Mater. Chem.* **2010**, *20*, 4937.
- [4] J. H. Yu, G. C. Rutledge, *Electrospinning*, in *Encyclopedia of Polymer Science and Technology*, John Wiley & Sons, Inc., **2002**.
- [5] D. Li, Y. Xia, *Adv. Mater.* **2004**, *16*, 1151.
- [6] S. Agarwal, J. H. Wendorff, A. Greiner, *Polymer* **2008**, *49*, 5603.
- [7] J.-J. Wang, L.-X. Dai, Q. Gao, P.-F. Wu, X.-B. Wang, *Eur. Polym. J.* **2008**, *44*, 602.
- [8] W.-Zhang, Y.-Wang, C.-Sun, *J. Polym. Res.* **2007**, *14*, 467.
- [9] I. S. Chronakis, *J. Mater. Proc. Technol.* **2005**, *167*, 283.
- [10] N. J. Pinto, A. T. Johnson, A. G. MacDiarmid, C. H. Mueller, N. Theofylaktos, D. C. Robinson, F. A. Miranda, *Appl. Phys. Lett.* **2003**, *83*, 4244.
- [11] D. Li, Y. Wang, Y. Xia, *Nano Lett.* **2003**, *3*, 1167.
- [12] W. E. Teo, S. Ramakrishna, *Nanotechnology* **2006**, *17*, R89.
- [13] C. Schramm, B. Rinderer, R. Tessadri, *J. Appl. Polym. Sci.* **2013**, *128*, 1274.
- [14] S. Chisca, A. I. Barzic, I. Sava, N. Olaru, M. Bruma, *J. Phys. Chem. B* **2012**, *116*, 9082.
- [15] F. Garnier, A. Yassar, R. Hajlaoui, G. Horowitz, F. Deloffre, B. Servet, S. Ries, P. Alnot, *J. Am. Chem. Soc.* **1993**, *115*, 8716.
- [16] Y. Shoji, R. Ishige, T. Higashihara, S. Kawachi, J. Watanabe, M. Ueda, *Macromolecules* **2010**, *43*, 8950.
- [17] W. J. Koros, G. K. Fleming, S. M. Jordan, T. H. Kim, H. H. Hoehn, *Prog. Polym. Sci.* **1988**, *13*, 339.
- [18] Google Patents (1965) invs.: R.H. William, Process for preparing polyimides by treating polyamide-acids with aromatic monocarboxylic acid anhydrides.
- [19] M. A. Kastner, *Rev. Modern Phys.* **1992**, *64*, 849.
- [20] B. R. Einsla, Y. Y. Hong, Y. S. Kim, F. Wang, N. Gunduz, J. E. McGrath, *J. Polym. Sci., Part A: Polym. Chem.* **2004**, *42*, 862.
- [21] J. D. Wind, C. Staudt-Bickel, D. R. Paul, W. J. Koros, *Macromolecules* **2003**, *36*, 1882.
- [22] N. Asano, M. Aoki, S. Suzuki, K. Miyatake, H. Uchida, M. Watanabe, *J. Am. Chem. Soc.* **2006**, *128*, 1762.
- [23] C. Huang, S. Chen, D. H. Reneker, C. Lai, H. Hou, *Adv. Mater.* **2006**, *18*, 668.
- [24] F. Chen, X. Peng, T. Li, S. Chen, X.-F. Wu, D. H. Reneker, H. Hou, *J. Phys. D: Appl. Phys.* **2008**, *41*, 025308.
- [25] Z.-M. Huang, Y. Z. Zhang, M. Kotaki, S. Ramakrishna, *Compos. Sci. Technol.* **2003**, *63*, 2223.
- [26] J. M. Deitzel, J. Kleinmeyer, D. Harris, N. C. Beck Tan, *Polymer* **2001**, *42*, 261.
- [27] L. Ji, A. J. Medford, X. Zhang, *Polymer* **2009**, *50*, 605.
- [28] D. Zhang, R. Chung, A. B. Karki, F. Li, D. P. Young, Z. Guo, *J. Phys. Chem. C* **2009**, *114*, 212.
- [29] D. Papkov, Y. Zou, M. N. Andalib, A. Goponenko, S. Z. D. Cheng, Y. A. Dzenis, *ACS Nano* **2013**, *7*, 3324.
- [30] V. Beachley, X. Wen, *Mater. Sci. Eng., C* **2009**, *29*, 663.
- [31] A. Tabe-Mohammadi, J. P. G. Villaluenga, H. J. Kim, T. Chan, V. Rauw, *J. Appl. Polym. Sci.* **2001**, *82*, 2882.
- [32] J. Zhu, S. Wei, D. Rutman, N. Haldolaarachchige, D. P. Young, Z. Guo, *Polymer* **2011**, *52*, 2947.
- [33] D. A. Grabowski, C. Schmidt, *Macromolecules* **1994**, *27*, 2632.
- [34] P. S. Tin, T. S. Chung, Y. Liu, R. Wang, S. L. Liu, K. P. Pramoda, *J. Membr. Sci.* **2003**, *225*, 77.
- [35] P. M. McGuiggan, D. A. Grave, J. S. Wallace, S. Cheng, A. Prosperetti, M. O. Robbins, *Langmuir* **2011**, *27*, 1.
- [36] J. Z. Guo, B. Qiu, C. Xu, D. Sun, H. Qu, M. Guerrero, H. Yi, J. Guo, X. Zhang, Z. Luo, N. Noel, S. Wei, X. Wang, *ACS Sust. Chem. Eng.* **2014**.
- [37] S. Madaeni, N. Ghaemi, *J. Membr. Sci.* **2007**, *303*, 221.
- [38] D. Li, A. W. Neumann, *J. Colloid Interface Sci.* **1990**, *137*, 304.
- [39] D. Li, A. W. Neumann, *J. Colloid Interface Sci.* **1992**, *148*, 190.
- [40] D. B. Mahadik, A. V. Rao, A. P. Rao, P. B. Wagh, S. V. Ingale, S. C. Gupta, *J. Colloid Interface Sci.* **2011**, *356*, 298.
- [41] D. Y. Kwok, A. W. Neumann, *Adv. Colloid Interface Sci.* **1999**, *81*, 167.